Evaluation of the Table Mountain Ronchi Telescope for Angular Tracking

G. Lanyi, G. Purcell, and R. Treuhaft
Tracking Systems and Applications Section

A. Buffington
Center for Astrophysics and Space Sciences
University of California at San Diego

The performance of the University of California at San Diego (UCSD) Table Mountain telescope has been evaluated to determine the potential of such an instrument for optical angular tracking. This telescope uses a Ronchi ruling to measure differential positions of stars at the meridian. The Ronchi technique is summarized in this article, and the operational features of the Table Mountain instrument are described. Results from an analytic model, simulations, and actual data are presented that characterize the telescope's current performance. For a star pair of visual magnitude 7, the differential uncertainty of a 5-min observation is about 50 nrad (10 marcsec), and tropospheric fluctuations are the dominant error source. At magnitude 11, the current differential uncertainty is approximately 800 nrad (approximately 170 marcsec). This magnitude is equivalent to that of a 2-W laser with a 0.4-m aperture transmitting to Earth from a spacecraft at Saturn. Photoelectron noise is the dominant error source for stars of visual magnitude 8.5 and fainter. If the photoelectron noise is reduced, ultimately tropospheric fluctuations will be the limiting source of error at an average level of 35 nrad (7 marcsec) for stars approximately 0.25 deg apart. Three near-term strategies are proposed for improving the performance of the telescope to the 10-nrad level: improving the efficiency of the optics, masking background starlight, and averaging tropospheric fluctuations over multiple observations.

I. Introduction

A need for higher data rates and more compact spacecraft hardware has led the Deep Space Network to contemplate using optical communication for the deep-space missions of the next century [1]. As optical communication is implemented, optical tracking can also be expected to supplement or replace the radio methods now in use. This article explores the applicability of an optical telescope with a Ronchi ruling in the focal plane ("Ronchi telescope") to differential angular tracking of interplanetary spacecraft. In particular, to understand the error

sources that limit both current and ultimate performance, the limiting errors of the UCSD–Table Mountain instrument have been examined using both real and simulated data. The levels of photoelectron and tropospheric fluctuations are analyzed, and analytical models are compared with actual performance over a range of visual magnitudes.

Figure 1 shows schematically the essential features of a Ronchi ruling, which is an optical grating consisting of alternate parallel opaque and transparent lines precisely laid down on a polished glass substrate. Typically there are several line pairs per millimeter, and the widths of the opaque and transparent lines are comparable, if not equal. On a Ronchi telescope the ruling lies in the focal plane, and during a measurement the stars in the field of view move across the ruling at a uniform rate. This motion can be induced either by moving the ruling within the telescope, or by holding the entire telescope fixed and allowing the Earth's rotation to carry the field of view across the ruling. In either case, a detector placed behind the ruling will observe the intensity of starlight modulated periodically by the ruling, as shown on the right side of the figure. If the width of the lines is comparable to the size of the image, the modulation will be continuous and of near-maximum amplitude. A time series of intensity measurements will then contain maximum information about the position of the image on the ruling, in the direction perpendicular to the ruling lines. If two stars are in the field of view simultaneously, then analysis of both time series can give a precise estimate of the difference of the stars' coordinates in that direction. This analysis will be described in more detail in Section II.

There are only three telescopes currently using Ronchi rulings for astrometry. The following list summarizes their distinguishing characteristics:

(1) Allegheny Observatory [2,3]: Refractor. Telescope tracks to maintain a fixed field of view. Motorized ruling moves across the field in orthogonal directions to determine two coordinates. Masks ("platens") for each field transmit light from only selected stars. Dedicated detector for each star.

(2) Hipparcos spacecraft, launched August 9, 1989 [4,5]: Reflector. Rotating telescope with slowly variable rotation axis. Optics superimpose two fields 58 deg apart. Fixed ruling rotates with the telescope. Electronic image dissector isolates stars.

(3) UCSD–Table Mountain [6]: Reflector. Meridian-transit telescope rotates with the Earth, fixed ruling rotates with the telescope. Measures right ascension difference only. Field of view divided into 12 declination bands with separate detectors. No background masking.

Each design has advantages for particular applications. For spacecraft tracking, a combination of the features listed above would be ideal. As a minimum, such an instrument must be able to determine differential right ascension *and* declination, have a masking capability to block background stars, and be able to reach visual magnitudes, m_v, in the neighborhood of 11. Other desirable—albeit not altogether compatible—features include extreme optical and mechanical stability, a minimum number of parts that move during a measurement, and freedom from optical aberrations over a wide, flat field of view.

Two lines of reasoning support the requirement given above for m_v. First, current projections suggest that spacecraft communication lasers will have apertures of about 0.4 m and transmit 2 W at a wavelength of 0.5 μm.[1] Calculations similar to those described in [7] show that such a laser, transmitting from Saturn, would have an effective m_v of about 11 as seen on Earth. Second, tracking with a Ronchi telescope requires that a reference star be in the same field of view as the spacecraft laser. Suppose that the field of view is 0.5 square degree (as for the Table Mountain telescope) and that observations are required at the point in the ecliptic farthest from the galactic equator, at galactic latitude 60 deg. According to Allen [8], the average density of stars brighter than $m_v = 10$ at that latitude is 4.3 per square degree, and for $m_v = 11$, the density is 11 per square degree. With these parameters, the probability that a random field is empty to $m_v = 10$ is at least 0.12; but at $m_v = 11$, the probability is less than 0.01. Thus, both arguments lead to the conclusion that the telescope must ultimately operate at about $m_v = 11$.

In the material that follows, Section II describes the essential features of the Table Mountain telescope and summarizes the way in which data are collected and analyzed. Section III presents the results of error modeling, simulations, and data analysis that explore the telescope's current and potential capabilities. Finally, Section IV discusses several planned improvements in the design of the telescope that will enable it to approach its ultimate performance.

II. Instrumentation and Data Analysis

The telescope used in these measurements is a Newtonian meridian-circle instrument owned by the University of

[1] J. R. Lesh, personal communication, Communications Systems Research Section, Jet Propulsion Laboratory, May 1990.

California at San Diego and located at JPL's Table Mountain Observatory. Figure 2 is a cross section through the telescope barrel that shows its essential features. Light entering at the right travels down the tube and is reflected from the parabolic primary mirror (M1), which has a diameter of 32 cm and a focal length, F, of 2.443 m. The converging beam then returns to the right along the optical axis to a flat diagonal mirror (M2), which redirects it to the primary focal plane at the Ronchi ruling (R). At this point, the field of view has a diameter of 5 cm, corresponding to 1.2 deg on the sky. Stellar images at the edge of the field are dominated by coma and are about 60 microns long.

On the Ronchi ruling (see Fig. 1), there are 400 line pairs (transparent and opaque) oriented parallel to the declination (north–south) direction in the image. Transparent and opaque lines are equally wide, and the combined width of a line pair is $d = 125$ microns. Thus, each line pair subtends an angle on the sky of

$$\Phi_R = d/F = 10.5545 \text{ seconds of arc} \qquad (1)$$

During a measurement, the telescope and ruling remain stationary while the Earth's rotation carries stellar images across the focal plane at a mean angular rate of $\omega = 15.0411$ arcsec/sec at the celestial equator. As an image traverses the ruling perpendicular to the lines, its transmitted light is modulated with a period equal to the time required to cross a line pair. This interval, the Ronchi period, is consequently given by

$$\tau_R = \frac{\Phi_R}{\omega \cos\delta} \qquad (2a)$$

where δ is the apparent declination of the star. Substituting the values given above for Φ_R and ω yields

$$\tau_R = 0.70171/\cos\delta \text{ seconds of time} \qquad (2b)$$

In essence, the phase of this periodic response of the Ronchi telescope is used to determine the relative right ascension of a star. For example, if two stars at the same declination differ in right ascension by $\Phi_R/2$ seconds of arc, their response functions will be offset by half a Ronchi cycle, and the observed phase difference can be used to deduce the right-ascension difference.

In order to detect the modulated starlight that has passed through the Ronchi ruling, it is convenient to use a system of transfer optics (labeled M3, L1, L2, and L3 in Fig. 2) to reimage the star field at the secondary image plane R′. Cylindrical lens L3 produces stellar images that are tightly focused in declination, but diffused along their direction of motion across the field. At R′, a series of 13 razor-edged steel shims extends in the right ascension direction to separate the image into twelve 0.038-deg-wide declination bands or channels. Twelve Plexiglas light pipes convey the light from each channel to a photomultiplier tube. The output current from each tube is then integrated in a capacitor, and the resulting voltage is sampled and digitized at intervals of $\Delta t = 0.075$ sec. Finally, the 12 counts collected for each sampling interval are recorded on a storage device, such as a magnetic disk, for later analysis.

Partitioning the field of view in this way makes it possible to distinguish and analyze separately the instrument's response to as many as 12 stars that are visible simultaneously. In general, of course, there will be several stars in each declination band at any given time, even though all of them may be faint. If the band contains a star to be measured, the cumulative effect of these background stars will influence the telescope's response and may be the dominant source of error. This error consists of two parts: The background stars increase the level of stochastic photoelectron noise, and also introduce systematic offsets in the estimated position as their response functions interfere with the response function of the star being measured. The background problem is discussed further in Sections III and IV.

As the foregoing discussion makes clear, the Ronchi telescope's response to a single star is a time series of photomultiplier counts (shown in Fig. 1) that rises and falls as the stellar image passes in turn across transparent and opaque lines of the Ronchi ruling. Because the width of the lines is comparable to the maximum coma-broadened size of a stellar image, the amplitude of the modulation is nearly 100 percent. The average number of sample points in a Ronchi period, N_R, is simply

$$N_R = \tau_R/\Delta t = 9.3562/\cos\delta \qquad (3)$$

Because N_R provides the most precise determination of focal length, the experimentally determined constant 9.3562 in Eq. (3) is used to calculate τ_R and Φ_R.

Optical stability, and mechanical and optical simplicity, were the primary considerations in the design of the Table Mountain telescope. Nothing moves during an observing session, and the absence of lenses in the primary optics minimizes chromatic aberration. The images do,

however, have the coma characteristic of a single parabolic mirror. As a result, the response function is not strictly periodic, and systematic errors can arise in the comparison of Ronchi phases measured at different points in the field of view.

Coma in the Table Mountain instrument is accounted for during data analysis. Buffington and Geller [6] argued that even in the presence of coma, the centroid of the image does move uniformly across the ruling. Furthermore, the centroid of a single peak in the response time series occurs when the centroid of the image crosses the midline of one of the transparent strips on the ruling. Hence, the problem of determining the phase of the Ronchi response function reduces to that of determining the centroid times of the response time series. That is, the analysis software computes for each peak in the response the centroid time,

$$\langle t \rangle_k = \frac{\sum_{i=1}^{n} t_i A_i}{\sum_{i=1}^{n} A_i} \tag{4}$$

where $\langle t \rangle_k$ is the time of the kth centroid, t_i is the ith sample time in the interval, and the values of A_i are the corresponding modulated intensities after removal of a background level that varies with time. The sum is taken over n data points in a particular peak.

In the absence of noise, the centroids of successive Ronchi cycles recur at equal intervals of τ_R, so that the Ronchi phase of the kth centroid can be defined as

$$\phi_k = (\langle t \rangle_k - t_{ref})/\tau_R - k \tag{5a}$$

where ϕ_k is in cycles and t_{ref} is a reference time common to all stars. Ronchi phase can be expressed as an angular offset in the right ascension direction simply by multiplying ϕ_k by the conversion factor Φ_R

$$\alpha_k = \Phi_R \phi_k \tag{5b}$$

Ideally, ϕ_k is constant for a particular star, but in the presence of perturbations (photoelectron noise, background stars, tropospheric refraction, and so on) it fluctuates. However, because the tropospheric fluctuations are correlated for stars separated by small angles, part of this error source cancels in a differential measurement between stars in different declination bands. Figure 3 shows the time series of Ronchi phase for a pair of magnitude-7 stars separated by about 23 minutes of arc. In the figure, the solid and dashed lines represent the phases of the two stars, and dots show the difference. To show the correlation of the tropospheric fluctuations more clearly, the mean phases of the two stars have been made equal. Because the troposphere is not the only source of error, and because the troposphere itself is not perfectly correlated, the correlation coefficient of the two time series is only about +0.5. In the following section, data on observed tropospheric fluctuations are presented, and the variation of photoelectron noise as a function of stellar brightness is discussed in detail.

III. Results

The goal in assessing the Table Mountain Ronchi telescope has been to evaluate the errors limiting its current performance and to determine how much that performance can be improved within the constraints imposed by its basic design. Ultimately, it will be necessary to decide whether such an instrument can track interplanetary spacecraft with the required accuracy. As discussed above, the two limiting error sources are photoelectron noise and tropospheric fluctuations.

In order to evaluate these two sources of error quantitatively, a combination of theoretical analysis, simulated data, and actual data has been used. Figures 4 and 5 summarize these results for differential observations of stars ranging from $m_v = 4.5$ to 12. In these figures, observed and calculated errors, in nanoradians, are plotted as a function of m_v.

Along the diagonal in Fig. 4, the solid line represents an analytic model of the component of angular error induced by photoelectron noise for the current instrument. The Appendix gives the derivation of this error for a single centroid measurement. To extrapolate the single-centroid calculation to a full-length (400-centroid) differential observation, a reasonable assumption was made that photoelectron noise on different centroids, or in different detectors, is statistically independent. Thus, the error on an average of 400 centroids is reduced by a factor of $\sqrt{400} = 20$ relative to a single centroid; and the error on a differential measurement is $\sqrt{2}$ times the error on a single-star measurement. Under this assumption, the plotted curve represents Eq. (A-9) divided by $\sqrt{200}$; that is,

$$\sigma_\alpha = (2089/A)(1 + 1.9604 \times 10^{-3} A)^{1/2} \tag{6}$$

where σ_α, the angular uncertainty, is expressed in nanoradians, $A = 10^{0.4(12-m_v)}$ is proportional to the star's brightness [see Eq. (A-8)], and m_v is its visual magnitude.

Note that the calculation of Eq. (6) (and the plotted line) assumes that the star is close to the celestial equator, where there are about nine sample points in a Ronchi period. Away from the equator, σ_α varies as $\sqrt{\cos\delta}$, where δ is the declination [see Eqs. (3) and (A-7)].

The six diamonds plotted in Fig. 4 represent actual differential measurements on six pairs of stars. Table 1 lists the stars in each pair, in order from left to right on the plot, along with their visual magnitudes and angular separations. For each pair, the plotted magnitude is an effective magnitude that accounts for the difference in magnitude of the two stars and the actual spectral response of the photomultiplier tubes.

The results for pairs 1 through 4 are derived from data collected on seven nights between May 23 and June 2, 1990. For each pair, the rms variation over the seven nights of the single-centroid differenced Ronchi phases was first calculated. Then, the single-centroid standard deviations were scaled to the length of a full observation by dividing by 20, as described above. This procedure implicitly assumes that the tropospheric, as well as the photoelectron, fluctuations scale with time as $t^{-1/2}$. Lindegren's semitheoretical estimate of differential tropospheric fluctuations [9] implies that this relation is correct, although his results do not strictly apply to the combination of angular separation (3 to 25 arcmin) and time interval (τ_R approximately 0.7 sec) applicable here. However, for undifferenced measurements, Lindegren [9] and his references expect the fluctuations to scale like $t^{-\beta}$, where β is between 1/6 and 2/5.

At the right in Fig. 4, the points for the two brightest pairs were obtained indirectly, by extrapolating the data given by Buffington and Geller [6] in their Fig. 5. That figure, based on five nights of measurements made from June 9 to June 13, 1989, shows angular precision as a function of integration time. Here their results have been extended to an integration time of 300 sec, assuming the $t^{-1/2}$ dependence suggested by the plot for shorter integration times.

Examination of the points shows that the weakest pairs lie near the theoretical photoelectron noise curve, but that, for brighter stars, the predicted photoelectron noise increasingly underestimates the actual angular uncertainty. Thus, it appears that for stars weaker than visual magnitude 8.5, photoelectron noise is the dominant error source. At magnitude 7.5, photoelectron and tropospheric fluctuations contribute about equally. For stars brighter than $m_v = 7$, the troposphere dominates the error budget. In Fig. 4, the rightmost points suggest that the error has nearly reached the asymptotic level of the tropospheric contribution alone. The horizontal line at about 35 nrad indicates an empirical estimate of that limit (for a single measurement) based on the data shown in the figure. Of course, this limit is merely representative. It depends on angular separation and on the time and place of the measurements.

Finally, the sloping line at the lower left in Fig. 4 shows the reduction in photoelectron noise expected to result from two improvements in telescope design discussed more fully in Section IV. First, masks are used to block background stars and remove their contribution to the noise; and second, the efficiency of the transfer optics and light pipes is improved by a factor of 12, so that the signal-to-noise ratio (SNR) increases by a factor of $\sqrt{12}$. With these improvements, the troposphere will dominate the error budget even at $m_v = 12$.

Figure 5 shows again the computed angular error due to photoelectron noise, and compares it with the results of tests in which the existing analysis software was used to process simulated data. In these tests, 1200 undifferenced 400-centroid observations were simulated at each of 16 visual magnitudes ranging from 4.5 to 12 in steps of 0.5. Gaussian noise representing photoelectron (but not tropospheric) fluctuations was added to a sinusoidal approximation of the Ronchi response function, and the results were written to a file in the same format as real data. The analysis software was then used in the usual way to compute an angular coordinate for each observation. Finally, each observation was assigned an error equal to the difference between the computed coordinate and the model coordinate used to generate the sinusoid. The plotted values along the solid line show the standard deviation of the 1200 errors, multiplied by $\sqrt{2}$ to account for differencing.

Except for the brightest and faintest stars, the predicted and simulated uncertainties agree remarkably well. It is not yet well understood why the simulations perform better than the model for stars of visual magnitude 12. The breakdown of the assumptions underlying Eq. (A-6) certainly plays a role, however. At the bright end of Fig. 5, it is suspected that an undiagnosed algorithm error is limiting the uncertainty derived from the simulated data at the 6-nrad level. If so, the simulation curve will agree better with the analytic model when the error is corrected.

Figure 6 applies the results shown in Fig. 4 to the special case of spacecraft tracking. As stated in Section I, a spacecraft laser with nominal characteristics at the distance of Saturn would generate a response in a Ronchi telescope comparable to that of a magnitude-11 star. Assuming a reference star of the same magnitude, the figure

shows the expected angular accuracy for several situations. At the left is shown the performance of the Table Mountain instrument, both in its current configuration and with the improvements mentioned above. On the right are the tropospheric errors for a single 5-min observation (taken from Fig. 4) and for the average of 25 statistically independent observations. With the expected improvements and multiple measurements, the estimated accuracy is adequate for near-term research and development demonstrations of optical astrometry.

IV. Conclusion

Very long baseline radio interferometric astrometry can now achieve an angular accuracy of 1 nrad or better [10]. Optical tracking methods must therefore strive toward a comparable goal. For ground-based systems in the near term, 10 nrad is a reasonable target. From the discussion in Section III, it follows that the Table Mountain telescope requires the improvements summarized below before it can deliver the desired performance.

For bright stars one or two tenths of a degree apart, tropospheric fluctuations typically limit differential accuracy to 30 or 40 nrad for a single 5-min measurement. Tropospheric error cannot be controlled, but it can be managed to some extent by observing at high altitude and using star pairs separated by small angles. It can also be reduced by averaging together several measurements, as indicated in Fig. 6.

For stars fainter than $m_v = 8.5$, photoelectron noise dominates the error budget. As pointed out in Section I, calculations of the apparent brightness of spacecraft lasers and of the number of observable stars lead to the conclusion that differential tracking measurements will have to rely on stars with m_v approximately 11. For such a pair (see Fig. 6), the differential angular uncertainty of a 5-min measurement with the current system is about 830 nrad.

Steps are already being taken that will reduce the photoelectron noise on stars of visual magnitude 11 to a level comparable to the tropospheric noise. An all-mirror Offner system [11] will replace the current lens system of transfer optics, increasing the telescope's optical transmission by a factor of 4. A further change in the way the light pipes are connected to the photomultipliers is expected to increase the number of photons that reach the detectors by another factor of 3. Since photoelectron noise varies as the square root of the incident intensity, this 12-fold increase in optical efficiency will increase the SNR by a factor of $\sqrt{12}$ and decrease the uncertainty of a measurement by the same amount.

Another factor that increases photoelectron noise is background light from fainter stars in each declination band. Typically, the total background in a band is comparable to the light from a magnitude-7 star. As mentioned in Section II, this background introduces both random and systematic errors into the estimated coordinates. To remove both kinds of errors, a masking device that will either block or ignore background light is being added. As a preliminary implementation, mechanical masks are being designed on at least two of the channels. Each mask will be an opaque strip that covers one declination band and contains a pinhole to allow only the light from a single star to pass. As the star crosses the field of view, a computer-controlled drive mechanism will move the mask to keep the star centered on the pinhole.

A much more versatile electronic masking system would use a sensitive charge-coupled device (CCD) to replace both the mechanical masks and the photomultiplier tubes. Such a system would retain the Ronchi ruling to modulate the starlight and would use the CCD as a masked detector. Only those CCD pixels containing the desired image would be processed, while those containing background would be discarded. A more radical departure from the current design would use the CCD not only to replace the masks and photomultipliers, but also as a metric device to replace the ruling itself. This pure CCD design may be subject to systematic errors that are difficult to control, however [12,13]. Although CCD's have been used in astrometry for over 10 years [14,15], the design envisioned here presents new challenges. In particular, it requires CCD's that are larger and can be read out faster than those now readily available. Thus, the CCD concept would be developed gradually only after a successful demonstration of mechanical masking.

Figure 4 shows the reduction in photoelectron error that is expected after the implementation of both background masking and improved transfer optics. With these improvements, the photoelectron error will be reduced below the tropospheric limit even for stars of visual magnitude 12.

Finally, tracking applications will require the measurement of spacecraft declination as well as right ascension. This capability can be added to the existing instrument in several ways. For example, stars would move obliquely across the ruling during observations made before or after transit. A pair or series of such observations could be combined to give a differential measurement of both right ascension and declination. Of course, this option would require modification of the telescope to allow nontransit measurements. Another approach would use a chevron

ruling with separate sections of lines oriented at ±45 deg with respect to the vertical. Still another possibility is to move the ruling itself in the declination direction, as Gatewood's instrument does [2,3]. Some of these methods are affected by differential atmospheric refraction, however, and it is still unclear what will be the best approach for two-dimensional measurements.

In summary, the following modifications would prepare the Table Mountain Ronchi telescope for a demonstration of its ability to track objects as faint as $m_v = 11$:

(1) Install the transfer optics now being developed, so as to improve the photoelectron SNR.

(2) Reconfigure the interface between the light pipes and the photomultipliers, which would also improve the photoelectron SNR.

(3) Design and install computer-controlled masks for at least two declination bands to eliminate the photoelectron noise and systematic errors caused by background stars.

The following two items offer some potential for improvement, but their feasibility has not yet been studied:

(1) Replace the photomultiplier tube assembly with a CCD (positioned so the image is slightly out of focus) to investigate the use of CCD's for both detection and masking.

(2) Install a Ronchi ruling with a chevron pattern for simultaneous measurement of right ascension and declination.

These improvements can be implemented on the current instrument with a modest investment, and they will make it possible to assess the applicability of the Ronchi technique to optical tracking.

References

[1] J. R. Lesh, L. J. Deutsch, and W. J. Weber, "A Plan for the Development and Demonstration of Optical Communications for Deep Space," *TDA Progress Report 42-103*, vol. July–September 1990, Jet Propulsion Laboratory, Pasadena, California, pp. 97–109, November 15, 1990.

[2] G. Gatewood, L. Breakiron, R. Goebel, S. Kipp, J. Russell, and J. Stein, "On the Astrometric Detection of Neighboring Planetary Systems," *Icarus*, vol. 41, pp. 205–231, February 1980.

[3] G. D. Gatewood, "The Multichannel Astrometric Photometer and Atmospheric Limitations in the Measurement of Relative Positions," *Astron. Journal*, vol. 94, pp. 213–224, July 1987.

[4] J. Kovalevsky, "Prospects for Space Stellar Astrometry," *Space Science Review*, vol. 39, nos. 1/2, pp. 1–63, September/October 1984.

[5] L. Lindegren, "Hipparcos Data Reduction Overview," *Adv. Space Research*, vol. 11, no. 2, pp. 25–34, 1991.

[6] A. Buffington and M. E. Geller, "A Photoelectric Astrometric Telescope Using a Ronchi Ruling," *Publications of the Astronomical Society of the Pacific*, vol. 102, no. 648, pp. 200–211, February 1990.

[7] B. L. Schumaker, "Apparent Brightness of Stars and Lasers," *TDA Progress Report 42-93*, vol. January–March 1988, Jet Propulsion Laboratory, Pasadena, California, pp. 111–130, May 15, 1988.

[8] C. W. Allen, *Astrophysical Quantities*, Third Edition, London: The Athlone Press, 1973.

[9] L. Lindegren, "Atmospheric Limitations of Narrow-Field Optical Astrometry," *Astron. and Astrophysics*, vol. 89, nos. 1/2, pp. 41–47, September 1980.

[10] R. N. Treuhaft and S. T. Lowe, "A Measurement of Planetary Relativistic Deflection," *Astron. Journal*, vol. 102, pp. 1879–1888, November 1991.

[11] A. Offner, "New Concepts in Projection Mask Aligners," *Optical Engineering*, vol. 14, no. 2, pp. 130–132, March/April 1975.

[12] A. Buffington, H. S. Hudson, and C. H. Booth, "A Laboratory Measurement of CCD Photometric and Dimensional Stability," *Publications of the Astronomical Society of the Pacific*, vol. 102, pp. 688–697, June 1990.

[13] A. Buffington, C. H. Booth, and H. S. Hudson, "Using Image Area to Control CCD Systematic Errors in Spaceborne Photometric and Astrometric Time Series Measurements," *Publications of the Astronomical Society of the Pacific*, vol. 103, pp. 685–693, July 1991.

[14] D. G. Monet and C. C. Dahn, "CCD Astrometry. I. Preliminary Results from the KPNO 4-m/CCD Parallax Program," *Astron. Journal*, vol. 88, pp. 1489–1507, October 1983.

[15] D. G. Monet, "Recent Advances in Optical Astrometry," *Ann. Rev. Astron. Astrophysics*, vol. 26, pp. 413–440, 1988.

Table 1. Star pairs shown in Fig. 4.

Pair	Stars (SAO identification)	Visual magnitudes	Separation, arcmin
1	122716, 122746	7.46, 8.20	24
2	122735, 122738	6.93, 8.40	13
3	122723, 122709	6.66, 7.60	14
4	122723, 122715	6.66, 7.22	23
5	70287, 70289	6.32, 6.49	3
6	101145, 101137	3.86, 5.91	13

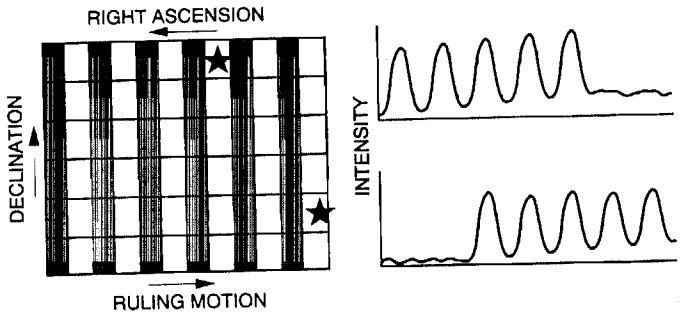

Fig. 1. Ronchi ruling: principle of operation.

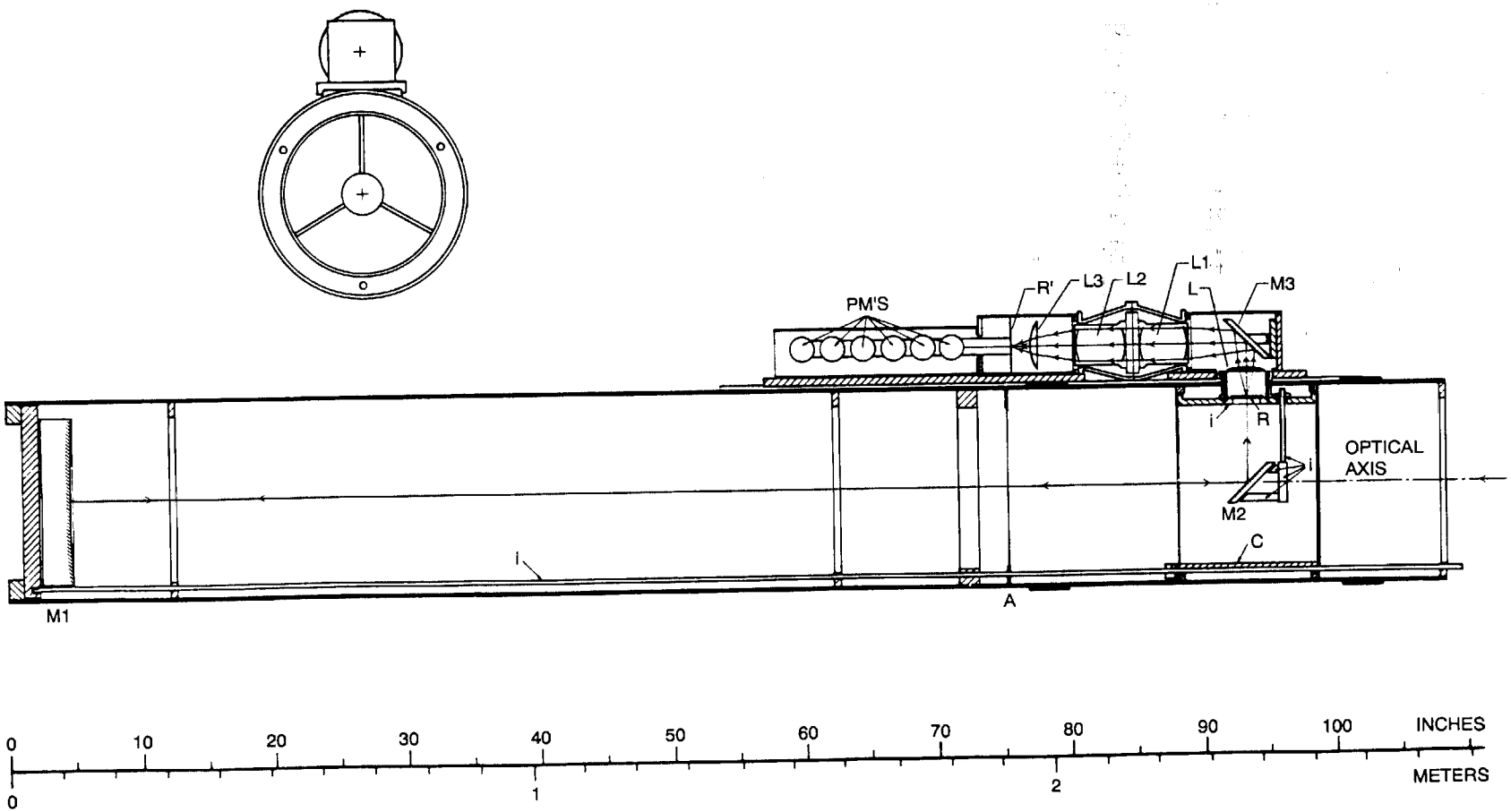

Fig. 2. Telescope configuration.

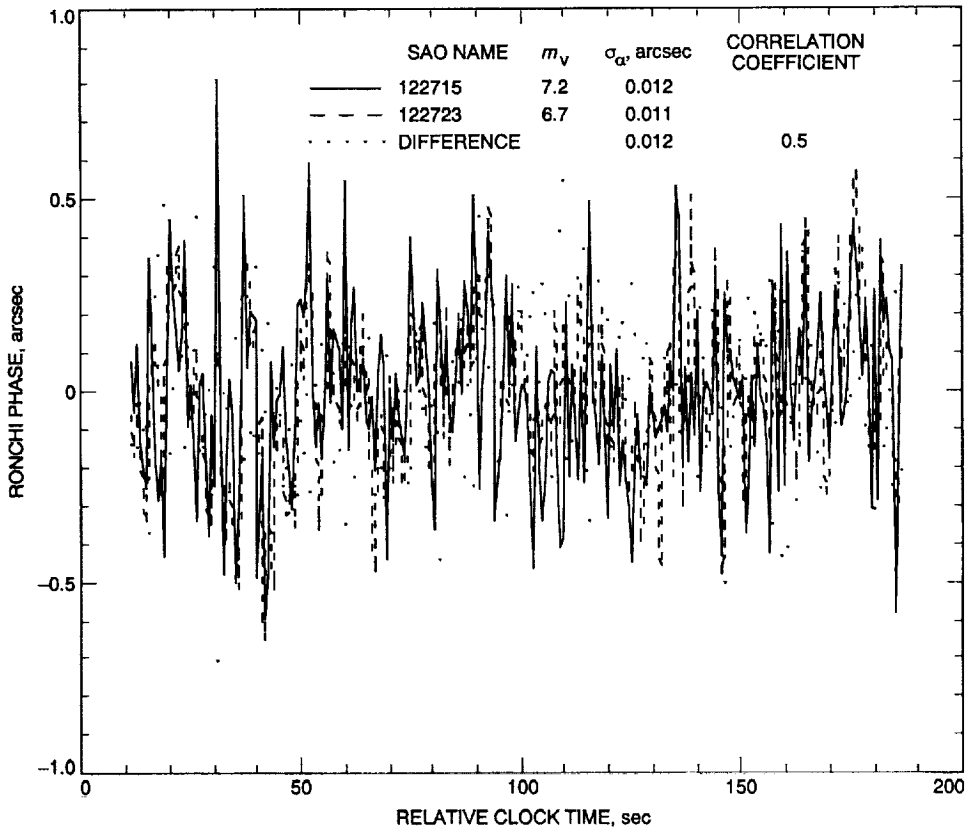

Fig. 3. Observed Ronchi phase.

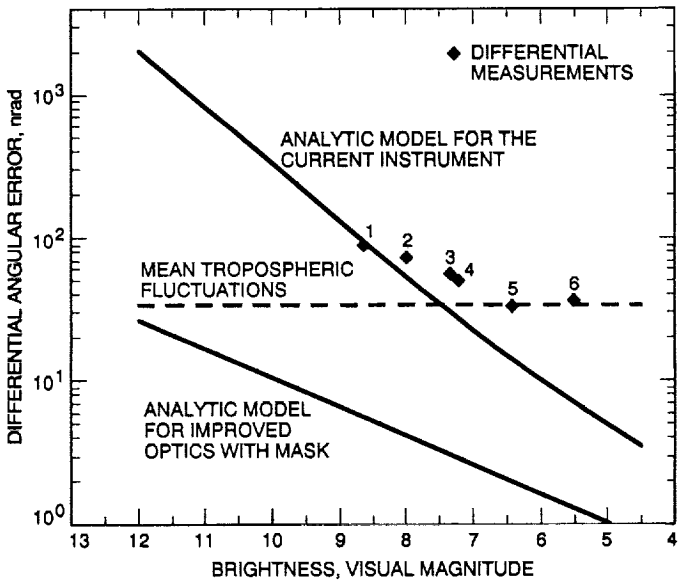

Fig. 4. Differential angular performance.

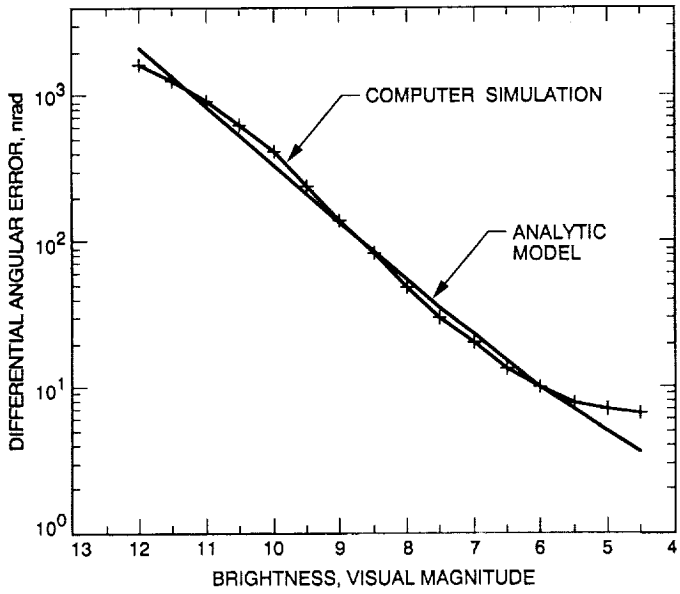

Fig. 5. Comparison of analytic error model with computer simulation. A relative uncertainty of 0.02 is associated with each simulated angular error value.

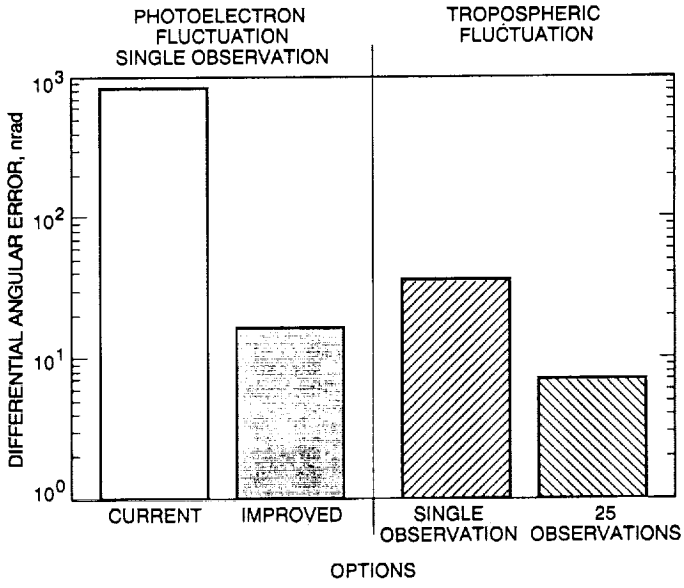

Fig. 6. Error budget for visual magnitude 11.

Appendix

Error in Estimate of Ronchi Centroid Caused by Photoelectron Fluctuations

In the Table Mountain Ronchi telescope, 12 analog-to-digital converters (ADC's) process the signals from 12 corresponding photomultipliers that have unequal gains. Where numerical constants are given below, they refer to channel 3. For other channels, the constants must be scaled by the appropriate gain ratio.

Since the response of each photomultiplier, A, is proportional to the number of photoelectrons, N, and N is proportional to the number of incident photons, the output from each ADC can be written as

$$A = KN \tag{A-1}$$

and is proportional to the brightness of the star being observed.

In the absence of a bright star in the field, there remains an average background level, A_B, due to faint stars. Even if the field of view remains fixed, this background has a stochastic fluctuation level (standard deviation), σ_B. From measurements of "empty" fields, the numerical values of these constants are found to be $A_B \approx 100$ and $\sigma_B \approx 3$. Since the standard deviation of the number of photoelectrons during any interval is the square root of the mean number during that interval (Poisson statistics), the fluctuation of Eq. (A-1) can be written as

$$\sigma = K\sqrt{N} \tag{A-2}$$

Thus, the value of K can be determined from the measured values of A_B and σ_B

$$K = {\sigma_B}^2/A_B \tag{A-3}$$

and from the values above, $K \approx 0.09$.

When the number of sample points in a Ronchi cycle is odd, $n = 2l+1$, the location of the centroid of the response function can be written as

$$x_c = (\Phi_R/n)\frac{\sum_{i=-l}^{l} iA_i}{\sum_{i=-l}^{l} A_i} \tag{A-4}$$

where the index i ranges over the points in a single Ronchi cycle, and x_c is expressed in the same units as Φ_R, the angle subtended on the sky by one Ronchi line pair [see Eq. (1)]. Note that the values of A_i in Eq. (A-4) are the amplitudes of the response time series of the single star being measured, after subtraction of the background level.

If the fluctuation of the amplitude, σ_i, is much smaller than the amplitude, A_i, then the variance of x_c is approximately

$$\sigma_{x_c}^2 = \frac{(\Phi_R/n)^2 \sum_{i=-l}^{l} i^2\sigma_i^2}{\left(\sum_{i=-l}^{l} A_i\right)^2} \tag{A-5}$$

where $\sigma_i = K\sqrt{N_B + N_{S_i}}$, and the subscripts B and S refer to the background and source, respectively. The value of N_B is more or less constant, but N_{S_i} varies directly with A_i. If the size of the stellar image on the Ronchi ruling is comparable to, or larger than, the line spacing, then the response function is roughly sinusoidal, and the response time series can be approximated as

$$A_i = \frac{A_S[1 + \cos(2\pi i/n)]}{2} \tag{A-6}$$

Using Eqs. (A-2), (A-3), and (A-6) in Eq. (A-5) and applying further numerical approximations, one obtains

$$\sigma_{x_c} = \frac{\Phi_R}{\sqrt{3n}}\sqrt{(\sigma_B/A_S)^2 + \frac{1}{2}(1 - 6/\pi^2)(\sigma_B/A_B)(\sigma_B/A_S)} \tag{A-7}$$

Measurements show that for a star of $m_v = 7$, $A_S \approx 100$, so that the relationship between signal amplitude and stellar magnitude is approximately

$$A = 10^{0.4(12-m_v)} \tag{A-8}$$

The approximations used in deriving Eq. (A-7) become significant for small values of n and A_S. For $n \geq 9$ (the smallest possible value) and $A_S \geq 30$ (corresponding to $m_v \approx 8$), the error is at most a few percent.

When one substitutes $n = 9$ for stars near the celestial equator, the numerical values given above for A_B and

σ_B, and the value of Φ_R from Eq. (1), then Eq. (A-7) becomes

$$\sigma_{x_c} = 2.03\sqrt{(3/A_S)^2 + (0.2)0.03(3/A_S)} \qquad \text{(A-9)}$$

where σ_{x_c}, the uncertainty in the location of the star caused by the photoelectron noise, is expressed in seconds of arc.

If the background is removed, only the second term in Eq. (A-9) remains

$$\sigma_{x_c} = 2.03\sqrt{(0.2)0.03(3/A_S)} \qquad \text{(A-10)}$$

Eq. (A-10) is correct within a few percent for stars brighter than $m_v \approx 11$. For stars fainter than the specified limits, Eqs. (A-7) and (A-10) both overestimate the actual uncertainties.